

Ligand Rebinding: Self-consistent Mean-field Theory and Numerical Simulations Applied to SPR Studies

Manoj Gopalakrishnan^{¶1}, Kimberly Forsten-Williams[§], Theresa R. Cassino[§], Luz Padro[§], Thomas E. Ryan[†] and Uwe C. Täuber[¶]

[¶] Department of Physics, Virginia Polytechnic Institute and State University,
Blacksburg, VA 24061-0435, USA.

[§] Department of Chemical Engineering and School of Biomedical Engineering and Sciences, Virginia Polytechnic Institute and State University, Blacksburg, VA 24061-0211, USA.

[†] Reichert, Inc., 3374 Walden Avenue, Depew, NY 14043, USA.

Key Words: Insulin-like growth factor-I (IGF-I), IGF Binding Protein-3 (IGFBP-3), Surface Plasmon Resonance, Optical Biosensor, Monte-Carlo Simulations

Running Title: Analysis of SPR Dissociation Studies

Abstract

Rebinding of dissociated ligands from cell surface proteins can confound quantitative measurements of dissociation rates important for characterizing the affinity of binding interactions. This can be true also for *in vitro* techniques such as surface plasmon resonance (SPR). We present experimental results using SPR for the interaction of insulin-like growth factor-I (IGF-I) with one of its binding proteins, IGF binding protein-3 (IGFBP-3), and show that rebinding, even with the addition of soluble heparin in the dissociation phase, does not exhibit the expected exponential decay characteristic of a 1:1 binding reaction. Within a self-consistent mean-field approximation, we derive the complete mathematical form for the fraction of bound ligand as a function of time and show that this function is non-exponential at all times, indicating that multiple rebinding events strongly influence dissociation even at early times. We compare the mean-field results with numerical simulations and find good agreement, although deviations are measurable in certain cases. Our analysis of the IGF-I-IGFBP-3 data indicates that rebinding is prominent for this system and that the theoretical predictions fit the experimental data well. Our results provide a means for analyzing SPR biosensor data where rebinding is problematic and a methodology to do so is presented.

¹ Present Address: Max Planck Institut für Physik komplexer Systeme, Nöthnitzer Straße 38, 01187 Dresden, Germany.

1. Introduction

Signal transduction via transmembrane receptor proteins is initiated by extracellular binding with specific proteins known as growth factors. These interactions tend to be of high affinity and, in many systems, are regulated by binding proteins present in the extracellular environment. Insulin-like growth factor-I (IGF-I) constitutes one prominent example of such a growth factor. Cell signaling is transmitted by direct interaction with the IGF-I receptor but this binding can be impacted by solution and cell-association IGF binding proteins (IGFBPs), of which there are at least six. Quantification of the interactions of IGF-I with IGFBPs is critical if one is to understand how changes in expression and secretion will impact IGF-I signaling. Surface plasmon resonance (SPR) is one technique amenable to such measurements. SPR is an optical sensor technique that has the advantage of being able to take real-time measurements using low concentrations of unlabeled biologicals [reviewed in Cooper, 2003].

Quantification of IGF-I interactions with both cell surface receptors and IGFBPs using SPR has been performed as a means of evaluating and predicting the competition between these molecules for IGF-I. Studies have used immobilized IGF-I [Wong et al., 1999; Dubaquié and Lowman, 1999; Galanis et al., 2001; Fong et al., 2002; Vorwerk et al., 2002], IGF-I receptor [Jansson et al., 1997], or IGFBPs [Heding et al., 1996; Jansson et al., 1997; Marinaro et al., 1999; Fong et al., 2002; Vorwerk et al., 2002] using amine chemistry to link the proteins to a carboxymethyl dextran (CMD) layer on the SPR chip. Deviations from a single reversible binding model have been noted and attributed primarily to non-uniform coupling of the ligand to the gel. Fong *et al.* (2002) compared kinetic parameters for IGF-I and IGFBP-1 using both a CMD and a self assembled monolayer (SAM) chip and saw significant differences in derived binding affinities that they attributed to possible steric hindrance effects and transport issues. Vorwerk *et al.* (2002) used a CMD chip with coupled IGFBP-3 and measured values that differed from previous work [Heding et al., 1996; Wong et al., 1999; Galanis et al., 2001; Fong et al., 2002] that they attributed to the use of increased flow rate to assist in combating mass transport and rebinding effects. However, regardless of flow rate, fitting of dissociation data for this system has been problematic.

A phenomenon of particular interest in the quantification of ligand interactions is rebinding: a ligand, following dissociation from a bound protein on the surface, may diffuse in the extracellular fluid environment for some time and may be reabsorbed later at one of the free binding sites. Rebinding is believed to be an important mechanism in producing cellular response, especially in dilute ligand concentrations, by assisting receptor proteins to stay in the active state for longer periods of time. Rebinding also may promote co-operative behavior among clustered receptors by reducing overall ligand dissociation, a phenomenon observed recently in experiments addressing the role of clustering in lipid rafts [Chu et al., 2004].

From a more general perspective, a quantitative characterization of the effects of rebinding is important in experiments like SPR, where dissociation rates of growth

factors (or other ligands) are measured. In such a situation, it would be ideal to eliminate rebinding altogether since it interferes with the measurement of dissociation and might lead to imprecise and significantly reduced dissociation rates [Nieba et al., 1995]. Low surface coverage and higher flow rates are techniques used to counteract mass transport limitations [Schuck, 1997]. Further, inclusion of specific proteins or molecules that may be used to bind to the released ligands or un-occupied binding sites and thus make them unavailable for rebinding is another technique targeted specifically at the rebinding problem. This technique has been used successfully for measuring the interaction of the SH2 domain of Ick with a phosphotyrosine peptide [de Mol et al., 2000]. However, in the absence of quantitative information on the affinity of these agents for binding to either the ligand or the receptor, it is difficult to estimate the general reliability of these methods. An alternative might be to understand how much rebinding might alter the dissociation of ligands in a given environment, and use this information to estimate the intrinsic rate of dissociation.

Rebinding of dissociated ligands has been studied previously using coupled partial differential equations for the time evolution of the probabilities with appropriate boundary conditions at the surface [Lagerholm and Thompson, 1998]. Although various quantities such as the rebinding probability of a released molecule could be calculated within this formalism, none of these could be compared directly with experimental results. By contrast, our mean-field theory, which is essentially based on well-known results from the theory of one-dimensional random walks, leads to a mathematical expression for the fraction of bound ligands (or receptors), which can be directly compared with SPR experiments.

In this paper, we present results of SPR experiments to measure dissociation of IGFBP-3 from IGF-I, and analyze these results using a mean-field analysis as well as Monte Carlo simulations. The SPR experiments are performed (i) in the presence and absence of flow conditions (ii) with and without addition of soluble heparin in the dissociation phase to bind released IGFBP-3 in solution, and (iii) with varying surface coverage of IGF-I. On the mathematical side, we first study the problem within a mean-field approximation (i.e., assuming a homogeneous distribution of receptors on the adsorption surface) and derive the complete form of the dissociation curve. We show that the dissociation in the presence of rebinding is non-exponential at all times (including very early times). We perform numerical simulations using a lattice model and compare the results with the mean-field prediction. The agreement is excellent, in general, but deviations from mean-field theory are measurable when high surface coverage of receptors is used. Our predictions are then checked against experimental dissociation curves, both in the presence and absence of exogenous heparin that binds to IGFBP-3 but not IGF-I [Forsten et al., 2001]. The mean-field dissociation function is found to fit the curves well up to time scales ~ 200 -300 seconds, at which time the finite height of the experimental system appears to become manifest with the effect of increasing the rebinding and thus further slowing down the dissociation.

This paper is divided into the following sections. In Sec. 2, we describe the SPR experimental setup and results. In Sec. 3, our self-consistent mean-field theory is

presented in detail and the mathematical form for the full dissociation curve is obtained in that framework. We then analyze the data by means of the mean-field function. Sec. 4 is concerned with the simulation model and the numerical results. We summarize this work and our findings in Sec. 5.

2. SPR experiments: description and results

2.1 Surface preparation

The surfaces used for these studies were composed of a mixed self assembled monolayer (mSAM) on gold (500 nm) coated slides (EMF Corporation, Ithaca, N.Y.) prepared as previously described [Lahiri et al., 1999] Briefly, the gold coated slides were immersed in a mixture of 0.2 mM carboxylic acid-terminated thiol and 1.8 mM tri(ethylene glycol)-terminated thiol (Toronto Research Chemicals, Toronto, Canada) for 12 hours. The surfaces were then rinsed with ethanol and dried under nitrogen. The resulting surface had free carboxyl groups for amine coupling and polyethylene glycol to minimize non-specific binding (Figure 1A).

2.2 Activation and immobilization:

Activation of the surface was achieved using N-ethyl-N-(3-diethylaminopropyl) carbodiimide (EDC) and N-hydroxysuccinimide (NHS) chemistry. Immobilization was done both on-line and off-line. Briefly, off-line immobilization was initiated by washing the chip surface with 20 mM NaOH and rinsing with phosphate buffered saline with 0.005% Tween, pH 7.4 (PBST) (Sigma-Aldrich Corp., St. Louis, MO). A fresh solution of 0.2 M EDC (Pierce, Rockford, IL) and 5 mM NHS (Aldrich Chemical Co., Milwaukee, WI) was placed on the surface of the slide and allowed to react for 12 min at room temperature. The chip was then rinsed with 20 mM sodium acetate, pH 5.5. IGF-I (PeproTech, Inc., Rocky Hill, New Jersey) was then immobilized by placing 0.2 ml of 3.3 μ M IGF-I in 20 mM sodium acetate solution onto the surface and incubated overnight in a container sealed under nitrogen at 4 °C. Following a wash with PBST, the slide was rinsed with 1M ethanolamine and then deactivated by surface exposure to 1M ethanolamine for 10 min at room temperature. The surface was then washed several times with PBST and dried with nitrogen prior to placing on the SPR unit.

On-line immobilization was performed in a similar fashion. Briefly, after placing the chip on the sensor surface, on-line immobilization was initiated by washing the chip surface with deionized water and then switching to PBST for ~5 min. until a stable baseline SPR signal was obtained. EDC/NHS solution (0.2 M EDC and 5 mM NHS in deionized water) was then injected into the system to activate the surface and allowed to react for 10 min. 20 mM sodium acetate buffer (pH 5.5) was then run over the sensor surface for ~ 5 min. until a stable baseline was obtained. IGF-I was then immobilized by running 3.3 μ M IGF-I in 20 mM sodium acetate solution over the surface for a particular amount of time to obtain the amount of IGF-I desired on the surface. PBST was then run for 4 min. to wash the surface. Following the PBST wash, 1M ethanolamine was run for 10 min. to deactivate the surface and prevent covalent

binding of other proteins to the slide. The surface was then washed with 20 mM HCl and 20 mM NaOH for 5 minutes each before switching to PBST for the binding experiments. The entire procedure was carried out at 25°C (controlled by the SPR instrument).

2.3 Dissociation experiments

Dissociation experiments were performed on a Reichert, Inc. SR 7000 Alpha instrument (Buffalo, New York) following either off-line immobilization of IGF-I and chip placement on the unit or on-line immobilization of IGF-I. PBST was run over the sensor surface and then followed by washes with 20mM HCl and 20 mM NaOH for 5 min each. The system was returned to PBST until a stable baseline was obtained (< 10 minutes) at a flow rate of ~0.8 ml/min. IGFBP-3 (Upstate Biotechnology, Lake Placid, NY) was pumped over the surface for 15 min to allow association. Following the association phase, PBST or PBST with heparin sodium from porcine intestinal mucosa (Celsus, Cincinnati, OH) was pumped over the surface to promote dissociation of the bound IGFBP-3. The surface was regenerated using 5 min washes of 2M NaCl in PBST, 20 mM HCl, and 20 mM NaOH. This procedure was repeated for each sample. Verification that the heparin sodium did not bind the IGF-I surface at the concentrations used for dissociation was performed.

2.4 Experimental results

Introduction of IGFBP-3 into the flow chamber over immobilized IGF-I led to the anticipated increase in binding characterized by a change in refractive index which is measured as pixels for the SR7000 Alpha unit, a similar unit to the RU commonly reported for the Biacore system (Figure 1B). The data was fit well by a 1:1 binding model with R^2 values of ~0.99 suggesting that heterogeneity of immobilized IGF-I was not a significant issue. The dissociation phase, however, did not reflect the exponential decay one would expect for a 1:1 binding interaction and global fitting using CLAMP [Myszka and Morton, 1998] either with or without mass transport did not provide a good fit (data not shown). Similar dissociation phase data were collected whether the system was under high flow or not (Figure 2A) despite some differences in the kinetics of association (data not shown) suggesting that rebinding might be a more prominent issue in the deviation from expected results for the dissociation phase. We have shown previously that IGFBP-3 and heparin interact strongly and negligible binding affinity was measurable between IGF-I and heparin, suggesting heparin might be a good rebinding inhibitor [Forsten et al., 2001]. Inclusion of heparin in the association phase significantly reduced IGFBP-3 binding levels while no change in pixels was observed when heparin was introduced to the IGF-I flow cell in the absence of IGFBP-3 (Figure 2B). We therefore investigated whether inclusion of heparin in the dissociation phase fluid would impact the dissociation rate. A significant reduction was observed (Figure 3) and was repeatable for both multiple runs on the same and on different chips and a heparin dose dependence effect was seen (data not shown). The reduction, while significant, still did not reflect exponential decay over the entire time regime. These experiments were all done however with off-line coupling of IGF-I to obtain high coverage, and consequently

good signal-to-noise, for our system. The SAM is designed with only 10% of sites available for binding although, depending on the radius of the protein, higher overall surface densities/coverage are possible [Lahiri et al., 1999] We therefore used on-line coupling to reduce coverage to see if that might impact dissociation. Ligand loading has been shown previously with CMD surfaces to impact interaction kinetic measurements [Edwards et al., 1997]. A reduction in IGF-1 surface coverage did result in somewhat faster dissociation particularly in the presence of high heparin concentrations but exponential decay was still not observed (Figure 4). Normalized association curves were not significantly different for the reduced coverage chips (data not shown).

3. Mean-field theory and Monte Carlo simulations

3.1 Self-consistent mean-field theory of ligand rebinding

In this section, we outline the mathematical theory of ligand dissociation and the consequent (multiple) rebinding to the binding sites on the surface. Let us consider a homogeneous distribution of receptor molecules (binding sites) on a two-dimensional surface with mean surface density P_0 per unit area. We define $p(t)$ to be the fraction of binding sites which are bound to ligands at time t , so that $p(0)$ is the fraction bound immediately following association. We denote the dissociation rate of ligands from the bound sites as β . The most general equation describing the time evolution of $p(t)$ is then

$$\frac{dp(t)}{dt} = -\beta p(t) + \gamma(t) \quad (1)$$

where $\gamma(t)$ represents the rate (probability per unit time) that a certain binding site will (re)absorb a ligand at time t .

The basic stochastic event contributing to the rate $\gamma(t)$ is the dissociation of a ligand at a certain bound receptor during a certain time interval $[\tau; \tau + d\tau]$, where $\tau < t$, and its subsequent adsorption at the reference site at time t . Our first simplification is to view the two-dimensional substrate surface as a (square) lattice of randomly mixed potential binding sites (depending on occupancy) and non-binding sites. We assume that the binding sites occur with a frequency

$$\theta \approx P_0 a^2 p_a \quad (2)$$

on the lattice, where a is the separation between two sites in the array (the typical inter-molecular spacing on the cell surface, say) and p_a is the adsorption probability (i.e., the probability that a ligand will be adsorbed on a free receptor upon contact). A second microscopic length scale is the typical separation between a bound receptor and its dissociated ligand immediately after dissociation). When the dissociated ligand is viewed as a Brownian particle in a dissipative medium, this length scale is the distance traveled by the particle before a significant change in its direction of motion takes place (i.e., the ‘diffusion’ length scale). We denote this length scale by Δ , which is discussed in more

detail in Sec.3.3. Within the mean-field approximation we employ here, the spatial fluctuations in receptor density are ignored, and the rebinding probability may be simply expressed as (see Appendix A for details)

$$\gamma(t) = \beta \int_0^t d\tau p(\tau) C_\theta(\Delta; t - \tau) \quad , \quad (3)$$

where $C_\theta(\Delta; T)$ is the probability that a diffusing particle starting at the point $z = \Delta$ at time $t = 0$ is adsorbed at $z = 0$ at $t = T$. In this formulation, the plane $z=0$ absorbs the particle with probability $\theta[1 - p(t)]$ and reflects it with probability $1 - \theta + \theta p(t)$. For further simplification, we assume that the initial bound fraction $p(0) \ll 1$, so that these probabilities are effectively time-independent. In this limit, rebinding of ligands is effectively reduced to a one-dimensional problem.

Equations 1 and 3 combined are formally solved using Laplace transforms. Let us define the Laplace-transformed variables $\tilde{p}(s) = \int_0^\infty p(t) e^{-st} dt$ and $\tilde{C}_\theta(s) = \int_0^\infty C_\theta(\Delta; t) e^{-st} dt$. In terms of these variables, Eq. 1, after substituting Eq. 3, becomes

$$s\tilde{p}(s) - p(0) = -\beta\tilde{p}(s) + \beta\tilde{p}(s)\tilde{C}_\theta(s)$$

which leads to

$$\tilde{p}(s) = \frac{p(0)}{s + \beta[1 - \tilde{C}_\theta(s)]} \quad (4)$$

The next step in our calculation is to compute $\tilde{C}_\theta(s)$, which we accomplish as follows: Let us consider a one-dimensional random walk on the semi-infinite line $0 < z < \infty$, and define $q(\Delta, t)$ as the probability that a random walker, starting at position $z = \Delta$ at time $t = 0$, will visit the origin again for the first time at instant t . The probability of absorption of the random walker at the origin at time t is $C_\theta(\Delta, t)$, which may be expressed in terms of $q(\Delta, t)$ via the following self-consistent equation:

$$C_\theta(\Delta, t) = \theta q(\Delta, t) + (1 - \theta) \int_0^t d\tau q(\Delta, \tau) C_\theta(\Delta, t - \tau) \quad (5)$$

The first term in this expression gives the probability that the ligand will be re-absorbed at its first attempt to make contact with the surface. The second term is the sum of the probabilities of all the other events where the ligand is reflected at the first attempt (either because the surface site is non-binding, or is already bound to another ligand), which may happen at any intermediate time τ , but is adsorbed at one of the subsequent attempts at time t . Using Laplace transforms as before, this expression becomes:

$$\tilde{C}_\theta(s) = \theta\tilde{q}(s) + (1 - \theta)\tilde{q}(s)\tilde{C}_\theta(s),$$

from which we infer

$$\tilde{C}_\theta(s) = \frac{\theta \tilde{q}(s)}{1 - (1 - \theta) \tilde{q}(s)} \quad (6)$$

The first passage probability for a random walker in one dimension is a well-studied problem with known result, namely: $q(z, t) = \frac{z}{t} \frac{1}{\sqrt{2\pi Dt}} e^{-\frac{z^2}{2Dt}}$ [Feller, 1966] for any $z > 0$ where D is the reduced diffusion coefficient for the three-dimensional random walk projected onto the z-axis. Upon performing the Laplace transform of this expression, we find that

$$\tilde{q}(s) = e^{-2\sqrt{\delta s}} \quad (7)$$

where we have introduced the quantity

$$\delta = \frac{A^2}{2D} \quad (8)$$

which constitutes a microscopic time scale in the problem. After substituting Eq. 7 into 6, we arrive at

$$\tilde{C}_\theta(s) = \frac{\theta e^{-2\sqrt{\delta s}}}{1 - (1 - \theta) e^{-2\sqrt{\delta s}}} \quad (9)$$

Note that this quantity vanishes in the limit $\theta \rightarrow 0$ since adsorption becomes rare in this case. This means that, in principle, rebinding can be effectively prevented and exponential dissociation recovered in the limit of extremely low surface coverage and/or very small absorption probability. However, for typical dissociation rates, this regime is difficult to reach experimentally (see Appendix B for a more detailed discussion).

With Eq. 9, we have, in principle, solved the rebinding problem under the mean-field approximation. However, the resulting general expression obtained after substituting Eq. 9 into Eq. 4 is too complicated to invert to find the rebinding probability. Fortunately, without much loss of generality, we can assume that the microscopic length scale δ is sufficiently small (in comparison with $1/\beta$) so that the approximation $e^{-2\sqrt{\delta s}} \approx 1 - 2\sqrt{\delta s}$ can be used. With this simplification, we find that $1 - \tilde{C}_\theta(s) \approx (2/\theta)\sqrt{\delta s}$ (when $\theta \gg \beta\delta$; see Appendix B). After substituting this expression into Eq. 4, we arrive at the final result

$$\tilde{p}(s) = \frac{p(0)}{s + \beta \frac{2}{\theta} \sqrt{\delta s}} \quad (10)$$

We note from this expression that the readsorption events have strongly modified the dissociation curve. In the absence of rebinding, this expression would simply read $\tilde{p}(s) = p(0)/(s + \beta)$, which is just the Laplace transform of an exponential decay curve, $p(t) = p(0)e^{-\beta t}$. In other words, the effect of rebinding is not simply a reduction of the effective dissociation rate, but rather it leads to a non-exponential temporal decay of the bound fraction. This is explicitly seen after inverting Eq. 10, which yields

$$p(t) = p(0)e^{ct} \operatorname{erfc}(\sqrt{ct}) \quad , \quad \text{where} \quad c = \frac{4\beta^2 \delta}{\theta^2} \quad \text{and} \quad \operatorname{erfc}(z) = \frac{2}{\sqrt{\pi}} \int_z^\infty e^{-x^2} dx \quad (11)$$

This final expression is thus characterized by a single effective time scale $1/c$, which is proportional to the inverse of the square of the dissociation rate. We also note that, within the limitations of the mean-field approximation and the assumptions used so far, Eq. 11 constitutes a complete solution of the rebinding problem, and not just an asymptotic one valid only for large times. We further note that even for very early times ($t \ll 1/c$), the solution does not become exponential. Rather, after applying the small argument expansion of the complementary error function [Abramowitz and Stegun, 1970] [$\operatorname{erfc}(z) \cong 1 - (2/\sqrt{\pi})z + o(z^2)$], we recognize that $p(t) \approx p(0)[1 - (4\beta/\theta\sqrt{\pi})\sqrt{\delta t} + \dots]$, i.e. the early-time behavior is algebraic and may be viewed as an expanded stretched exponential. For very late times ($t \gg 1/c$), the decay actually becomes a power law, i.e., $p(t) \sim 1/\sqrt{t}$. This regime is indeed observed in simulations when a very low value of the coverage θ is used (c.f. Fig. 8 below).

We would also like to make a note on finite-size effects here, keeping in mind that our goal is a direct comparison with experimental results (to be discussed in Sec. 4). The experimental system has a finite ‘height’, so that dissociated ligands which wander too far from the adsorption surface are eventually reflected back. This effect of the boundary will be seen in the dissociation curve after a certain cross-over time scale, which we estimate as typically, $\tau_H \sim H^2/(2D)$ where H is the sample chamber height. The presence of the boundary thus leads to additional rebinding events (as compared with the idealized case of infinite H studied so far), and slows down dissociation even more relative to our mean-field prediction over times $t \gg \tau_H$. This deviation from the infinite-height mean-field prediction is indeed observed in the experiments (Sec. 4). An extension of the present study that takes the finite height of the experimental system into account is currently under study.

3.2 Lattice model of ligand-receptor binding

In order to check the results from the self-consistent mean-field approximation, we next describe a discrete lattice model amenable for simulating the rebinding problem. As mentioned in the introduction to the last section, we imagine the cell surface as a two-dimensional square lattice of dimensions $L \times L$. A fraction θ of the lattice sites are occupied by receptor proteins, i.e., they serve as potential binding sites for the ligand.

The remainder of the sites are non-binding: the ligands, upon contact with one of these, will be reflected back to the solution. The ligands themselves are modeled as Brownian particles (random walkers) diffusing in the semi-infinite 3-dimensional space, of which the cell surface forms one (partially absorbing) boundary. Periodic boundary conditions are imposed on all four borders of the two-dimensional lattice so that a ligand that exits at one boundary will reenter the system from the opposite one. The direction perpendicular to the plane of the lattice shall be referred to as the z-axis, and the surface itself is positioned at $z=0$. Ligand diffusion in the z-direction is not bounded. We also neglect surface diffusion of the receptor proteins and treat them as static in this present study. The lattice dimension is fixed at $L=100$ for all the simulations reported in this paper.

At the beginning of the dynamics, a fraction $p(0)$ of all the binding sites are bound to a ligand each, i.e., the total number of ligands in the system is $N=L^2\theta p(0)$, and is conserved throughout the simulation. There are three main dynamical processes in the simulation:

- (i) Dissociation of a ligand from a bound receptor: this process takes place with probability $\tilde{\beta}$ (we use a different symbol to distinguish from the variable used in the last section) per time step. This move updates the position of the ligand from $z=0$ to $z=2$. (We set $z=2$ instead of $z=1$ in order to prevent immediate rebinding to the same receptor.)
- (ii) Diffusion of a released ligand in solution: a free ligand moves a distance equal to one lattice spacing in one of the six possible directions (i.e., to nearest-neighbor sites in the cubic lattice) with probability $\tilde{D}=1/6$ per time step.
- (iii) Readsorption of free ligand to a free receptor: A free ligand at $z=1$ (or correspondingly, $z=\Delta$ in the continuum theory of last section) is absorbed by a free receptor below it, if there is one present at that site, with probability p_a . We set this probability equal to 1 in most of the simulations reported here (i.e., the ligand-receptor binding is assumed to be purely diffusion-limited: the binding reaction always occurs when possible).

3.3 Parameters in the lattice model

In order to establish a close connection between the lattice model in our simulations and the underlying experimental system, it is necessary to put our choice of parameters on a firm footing. We begin with the microscopic length scale Δ , which we define as the distance moved by a ligand following dissociation, before a significant change in its direction of motion takes place. The time taken by the ligand to travel this distance is then simply equal to δ from Eq. 8. For a Brownian particle of mass m moving in a fluid of viscosity η , the velocity correlations decay exponentially fast: $\langle v(0)v(t) \rangle \propto e^{-t/\tau}$, where

$$\tau = m / 6\pi a\eta = Dm / 6kT \quad (13)$$

where we have used the Stokes-Einstein formula $D = k_b T / \pi \eta a$ to eliminate the ‘radius’ of the ligand molecule a in favor of the diffusion coefficient, which is generally estimated (based on the size of the molecule) to be of the order of $D \approx 10^{-6} \text{ cm}^2 \text{ s}^{-1}$ and the viscosity of water at room temperature; $\eta \approx 10^{-2} \text{ P}$. Following our previous argument, we may then define δ as the characteristic time scale for the decay of the velocity auto-correlations. Such an operational definition would yield $\delta \approx 10\tau$. After using the estimates for the mass of a ligand molecule ($m \approx 1000m_{\text{H}_2\text{O}}$), the diffusion coefficient D and the temperature ($T \approx 300\text{K}$), we find that

$$\delta \approx 10^{-12} \text{ s} \quad (14)$$

In the simulations, we also choose a dissociation rate per unit time step, $\tilde{\beta} \approx \beta \delta t$, where $\delta t = \lambda^2 / 6D = \delta / 3$ is the diffusion time scale. ‘Typical’ dissociation rates reported in the literature are quite small - for example, Vorwerk et al. estimated β for IGF-I-IGFBP-3 using SPR to be $\sim 0.01 \text{ min}^{-1}$ [Vorwerk et al., 2002] – meaning that $\tilde{\beta}$ will be very small, since δ is a microscopic time scale. In the simulations reported here, we have fixed $\tilde{\beta} = 10^{-5}$ to limit computational time, although a more realistic value of $\tilde{\beta}$ might be smaller by several orders of magnitude. For the simulations, starting from a randomly distributed set of receptors, the dynamics is carried out up to 10^7 Monte Carlo time steps (i.e., up to 100 times $1/\tilde{\beta}$). The bound fraction $p(t)$ is measured every 100 MC steps. The resulting dissociation curve is then averaged over 20 different starting configurations.

3.4 Simulation results

In Fig. 5, we show the (normalized) dissociation curve as obtained from the Monte Carlo simulations, for two values of θ , 0.1 and 0.5 respectively, plotted against the ‘scaled time’ $T = \tilde{\beta} t$ where t is the number of MC steps. The fraction of surface proteins initially bound to diffusible ligand was fixed at $p(0) = 0.25$. We find that, everything else being the same, larger θ results in stronger rebinding and hence slower dissociation. Since time is measured in units of β^{-1} , the effective fitting parameter becomes $c = 4\beta\delta / \theta^2 = 12\tilde{\beta} / \theta^2$. For $\theta = 0.1$ and 0.5, respectively, the theoretical fitting parameters are thus 0.012 and 0.00048. The measured values found using the best fits to the simulation data are very close, but somewhat smaller than these theoretical values. This slight discrepancy could be due to two factors: (i) the mean-field calculation assumes that all the surface proteins are available for rebinding at any given time, whereas in the simulations only free receptors are available; (ii) a systematic deviation from the mean-field prediction might exist, since (especially for high receptor density), local density fluctuations are likely to become important in the rebinding.

In Fig. 6, we show how the dissociation curves behave in the case of an extremely small fraction of binding sites ($\theta = 0.01$) on the surface, when the dissociation rate is varied. In this situation, two regimes are observed. When the dissociation rate $\tilde{\beta}$ is small, then

between two dissociation events, the ligand has enough time to span the surface for binding sites. The dissociation curve is thus dominated by rebinding, and a very slow decay in accordance with Eq. 11 is observed. Alternatively, when dissociation is very fast, rebinding is very inefficient in competing with dissociation because the fraction of binding sites is very small. The dissociation curve is, in this case, closer to the pure exponential dissociation curve in the absence of rebinding (see the discussion in Appendix B). A similar effect may be observed also by reducing the rebinding probability p_R while keeping the parameters θ and $\tilde{\beta}$ constant (data not shown).

In Figs. 7 and 8, the dissociation curves are depicted for two small values of the coverage fraction: $\theta=0.005$ and 0.01 , holding $\tilde{\beta}$ fixed at 10^{-5} . The logarithmic plots in Fig.8 show a cross-over to the power-law decay $p(t) \sim 1/\sqrt{t}$ discussed in the previous section. In our experimental system, however, such a cross-over behavior would be rather difficult to observe because finite size effects could disrupt and mask the entry into this regime.

4. Fitting the experimental data to the mean-field result

We observe that, except for very late times, all the data sets fit reasonably well with the theoretical prediction given by Eq. 11, with the parameter c suitably adjusted (Figs. 9 and 10). To see if the deviation from the theoretical curve could be caused by the finite height of the system (as discussed in the end of Sec. 3.1), we compute the cut-off time scale $\tau_H \sim H^2/(2D)$. For $H=0.19\text{mm}$ as in the SPR experiments and a ligand diffusion coefficient of $D \sim 10^{-6} \text{cm}^2 \text{s}^{-1}$, we find that $\tau_H \sim 300\text{s}$. From the experimental data, the estimate for τ_H ranges from $\sim 200 \text{ s}$ (no heparin present) to 300 s ($5.4\mu\text{M}$ heparin), which are quite close to the theoretical estimate.

The addition of heparin in the buffer leads to faster dissociation (Fig.10, also Table 1), and we observe a systematic increase in the fitting parameter c as the heparin level is increased. However, it is worth noting that an exponential decay is not recovered even with heparin concentrations as high as $10.8 \mu\text{M}$. This is all the more remarkable because the affinity of heparin for IGFBP-3 has been measured to be $\sim 76 \text{ nM}$ using affinity co-electrophoresis [Forsten et al., 2001]. In a well-mixed solution of heparin and IGFBP-3, the fraction of the free ligand in the steady state would be $p = 1/(1 + \rho/K_d)$, where ρ is the heparin concentration. For $\rho = 1.8 \mu\text{M}$ and $5.4 \mu\text{M}$ respectively, this fraction is only 0.04 and 0.01 (and similar values for the other heparin concentrations). If a steady state were indeed reached between heparin and the free ligand, we should see a corresponding change in the parameter θ since, presumably, only the ligand not bound to heparin will be available for rebinding (i.e., $\theta \rightarrow \theta_H = \theta p$). However, the change in θ as determined from the fitting parameter c is much less than this estimate noting that even at $10.8 \mu\text{M}$ heparin, about 15% of the ligand in solution are not bound to heparin and hence available for rebinding (Table 1).

We now attempt to estimate the actual dissociation rate β from our curve-fitting analysis. We start with the fit value $c = 1.9 \times 10^{-5} \text{ s}^{-1}$ for the heparin-free case (Fig. 7) and use the estimate of δ discussed in Sec. 3, Eqs. 13 and 14, which gives $\beta \approx 2291\theta \text{ s}^{-1}$. From Eq. 2, θ is the product of the surface coverage of receptors which was estimated to be approximately 10% or greater in this experiment based on the surface chemistry and the adsorption probability, which is unknown.

An estimate of the adsorption probability may be obtained as the ratio of the measured association rate to the purely diffusion-limited association rate. For the latter, we imagine the receptors as spherical objects of radius b , in which case the diffusion-limited association rate from Smoluchowski theory is simply $k_D = 4\pi bD$ [Torney and McConnell, 1983]. Since only the half-space above the surface is available for diffusion of the ligands, the diffusive flux is also halved, and hence, a better estimate would be $k_D \approx 2\pi bD$. The experimentally measured association rate for IGFBP-3 and IGF-I binding for our experimental system is $k_{exp} \cong 1.1 \times 10^7 \text{ M}^{-1} \text{ min}^{-1}$ [Cassino, 2002]. After using a realistic estimate, $b \sim 5 \text{ nm}$ for the receptor protein ‘radius’, we find that:

$$p_a = k_{exp} / k_D \approx 10^{-4} \quad (15)$$

For the dissociation rate, this analysis then gives $\beta \approx 0.02 \text{ s}^{-1}$. Note that because of possible errors in the estimates of parameters such as δ , θ , and p_a , this result is not necessarily quantitatively accurate. Rather, we view the fact that our estimate of the dissociation rate from this curve-fitting analysis does not differ significantly from typical values quoted in literature as supportive of the mathematical formalism we have presented here. Further characterization of the experimental system is necessary to obtain a more quantitative value.

5. Summary and discussion

In this paper, we present an experimental, analytical, and computational study of the dissociation of ligands from a flat substrate. We have especially focused on the role of potentially multiple rebinding of dissociated ligands, and how it affects the overall dissociation. The SPR experiments were done with IGFBP-3 as the soluble ligand and IGF-I attached to a planar surface as the receptor. Porcine heparin was used to bind the dissociated IGFBP-3 in solution, and its effect on the dissociation at various concentrations was studied.

The dissociation of IGFBP-3 was non-exponential in all the SPR experiments performed (Fig. 3) despite using a planar geometry surface (Fig. 1) to reduce mass-transport limitations known to be problematic with SPR experiments [Schuck, 1996; Schuck, 1997]. It should be noted, however, that similar non-exponential dissociation results were found by us [Cassino, 2002] and others [Wong et al., 1999; Dubaquié et al., 1999; Fong et al., 2002] using the more traditional carboxymethylated dextran slides with IGF-I

or IGFBP-3 immobilized. The addition of heparin was observed to render the dissociation faster, presumably by binding the dissociated IGFBP-3 and preventing their rebinding to unbound IGF-I. However, in no experiment did we actually observe actual exponential decay. This was true even for heparin concentrations as high as 30 μM indicating that equilibrium was not reached between heparin and IGFBP-3 over the experimental time scales. Simple fitting of an exponential to the dissociation data is, in general, not appropriate and a better tool is needed to determine quantitative values.

Our analysis, however, does not rule out the possibility of situations where an exponential fit to the dissociation curve might produce the right dissociation rate. As discussed in Appendix B, if the rebinding probability (i.e., the affinity of the receptor for the ligand) and/or surface coverage of receptors is small compared to the dissociation rate, the rebinding process simply appears as a small perturbation in the dissociation curve (ref. Eq. B3), and it may be possible to neglect it altogether. Alternatively, if the ligand has high affinity for an external binding agent, such as heparin in our system, then using this agent in sufficiently high concentrations might be successful in making rebinding insignificant as far as dissociation is concerned. Many examples are available in the literature where a simple model has been shown to fit well. For example, binding of interleukin-2 to a surface of IL-2 α -receptor surface was shown to fit well to a simple bimolecular model [Myszka, 1999]. Schuck et al. (1998) use competitive dissociation to obtain an improved fit for binding of a specific Fab to immobilized whale neuraminidase.

The self-consistent mean-field theory presented in this paper provides a complete mathematical form of the dissociation curve in the presence of rebinding, in terms of a single effective parameter. This effective parameter depends on the actual dissociation rate, the fraction of the surface area covered by binding sites, the probability of binding upon contact by diffusion, and the diffusion coefficient of the ligands in solution. As the formalism developed here yields the dissociation curve itself, we believe this to constitute a marked improvement over previous mathematical studies of rebinding [Lagerholm and Thompson, 1998], especially since our results could be directly compared with experiments.

Acknowledgements:

We thank D. Lubensky, R. Kree, T. Newman, H. J. Hilhorst and B. Schmittmann for fruitful discussions. Financial support from the National Science Foundation [NSF-DMR 0089451 (MG), NSF-DMR 0308548 (UCT), NSF-9875626 (KFW), Graduate Fellowship (TRC)] and the Bank of America Jeffress Memorial Trust [Grant no. J-594 (UCT)] is gratefully acknowledged.

References

Abramowitz, M. and I. A. Stegun. 1970. Handbook of Mathematical functions. Dover. New York.

Cassino, T.R. 2002. MS Thesis, "Quantification of the Binding of Insulin-like Growth Factor-I (IGF-I) and IGF Binding Protein-3 (IGFBP-3) using Surface Plasmon Resonance". Virginia Polytechnic Institute and State University. Blacksburg, Virginia

Chu, C.L., J.A. Buczek-Thomas and M.A. Nugent. 2004. Heparan sulphate proteoglycans modulate fibroblast growth factor-2 binding through a lipid raft-mediated mechanism. *Biochem. J.* 379:331-341

Cooper, M.A. 2003. Label-free screening of bio-molecular interactions. *Anal. Bioanal. Chem.* 377:834-842

de Mol, N.J., E. Plomp, M.J. Fischer and R. Ruijtenbeek. 2000. Kinetic analysis of the mass transport limited interaction between the tyrosine kinase lck SH2 domain and a phosphorylated peptide studied by a new cuvette-based surface plasmon resonance. *Anal Biochem.* 279:61-70

Dubaquie, Y., and H.B. Lowman. 1999. Total alanine-scanning mutagenesis of insulin-like growth factor I (IGF-I) identifies differential binding epitopes for IGFBP-1 and IGFBP-3. *Biochemistry* 38:6386-6396

Edwards, P.R., P.A. Lowe, and R.J. Leatherbarrow. 1997. Ligand loading at the surface of an optical biosensor and its effect upon the kinetics of protein-protein interactions. *J. Mol. Recogn.* 10:128-134

Erdelyi, A.(ed.). 1954. Tables of Integral Transforms. McGraw Hill. New York.

Feller, W. 1966. Introduction to Probability theory and applications Vol. 1. Wiley. New York.

Fong, C.-C., M.-S. Wong, W.-F. Fong, and M. Yang. 2002. Effect of hydrogel matrix on binding kinetics of protein-protein interactions on sensor surface. *Analytica Chimica Acta.* 456:201-208

Forsten, K.E., R. M. Akers and J. D. San Antonio. 2001. Insulin-like growth factor (IGF) binding protein-3 regulation of IGF-I is altered in an acidic extracellular environment. *J Cell Physiol.* 189:356-365

Galanis, M., S. M. Firth, J. Bond, A. Nathanielsz, A.A. Kortt, P.J. Hudson, and R.C. Baxter. 2001. Ligand-binding characteristics of recombinant amino- and carboxyl-terminal fragments of human insulin-like growth factor-binding protein-3. *J. Endocrinol.* 169:123-133

Heding, A., R. Gill, Y. Ogawa, P. De Meyts, R.M. Shymko. 1996. Biosensor measurement of the binding of insulin-like growth factors I and II and their analogues to the insulin-like growth factor-binding protein-3. *J. Biol. Chem.* 271:13948-13952

Jansson, M., J. Dixelius, M. Uhlen, and B.O. Nilsson. 1997. Binding affinities of insulin-like growth factor-I (IGF-I) fusion proteins to IGF binding protein 1 and IGF-I receptor are not correlated with mitogenic activity. *FEBS Lett.* 416:259-264

Lagerholm, B.C., and N. L. Thompson. 1998. Theory for ligand rebinding at cell membrane surfaces. *Biophys. J.* 74:1215-1228

Lahiri, J., L. Isaacs, J. Tien, and G. M. Whitesides. 1999. A strategy for the generation of surfaces presenting ligands for studies of binding based on an active ester as a common reactive intermediate: a surface plasmon resonance study. *Anal. Chem.* 71:777-790

Marinero, J.A., G.P. Jamieson, P.M. Hogarth, and L.A. Bach. 1999. Differential dissociation kinetics explain the binding preference of insulin-like growth factor binding protein-6 for insulin-like growth factor-II over insulin-like growth factor-I. *FEBS Lett.* 450:240-244

Myszka, D.G., and T.A. Morton. 1998. CLAMP: a biosensor kinetic data analysis program. *Trends Biochem Sci.* 23:149-150

Myszka, D.G. 1999. Improving biosensor analysis. *J. Mol. Recognit.* 12:279-284

Nieba, L., A. Krebber and A. Pluckthun. 1996. Competition BIAcore for measuring true affinities: large differences from values determined from binding kinetics. *Anal. Biochem.* 234:155-165

Schuck, P. 1997. Use of surface plasmon resonance to probe the equilibrium and dynamic aspects of interactions between biological macromolecules. *Ann. Rev Biophys Biomol Struct.* 26:541-566

Schuck, P., D.B. Millar, and A.A. Kortt. 1998. Determination of binding constants by equilibrium titration with circulating sample in a surface plasmon resonance biosensor. *Anal. Biochem.* 265:79-91

Schuck, P. 1997. Reliable determination of binding affinity and kinetics using surface plasmon resonance biosensors. *Curr. Opin. Biotechnol.* 8:498-502

Schuck, P. 1996. Kinetics of ligand binding to receptor immobilized in a polymer matrix, as detected with an evanescent wave biosensor. I. A computer simulation of the influence of mass transport. *Biophys. J.* 70:1230-1249

Torney, D.C and H. M. McConnell. 1983. Diffusion-limited reaction rate theory for two-dimensional systems. Proc. R. Soc. London, Ser. A. 387: 147-170.

Vorwerk, P., B. Hohmann, Y. Oh, R.G. Rosenfeld, and R.M. Shymko. 2002. Binding properties of insulin-like growth factor binding protein-3 (IGFBP-3), IGFBP-3 N- and C-terminal fragments, and structurally related proteins mac25 and connective tissue growth factor measured using a biosensor. *Endocrinology* 143:1677-1685

Wong, M. -S., C.-C. Fong, and M. Yang. 1999. Biosensor measurement of the interaction kinetics between insulin-like growth factors and their binding proteins. *Biochim. Biophys. Acta.* 1432:293-301

Appendix A

Let us consider the bulk diffusion of a free ligand in three dimensions, starting at the point (x, y, z) at time $t = 0$ and arriving at $(0, 0, Z)$ at $t = T$. The probability density for this process will be denoted by $P(x, y, z; T)$; it is governed by the diffusion equation modified by a term to account for surface adsorption,

$$P(r, t + \delta t) - P(r, t) = \tilde{D}[\sum_{r'} P(r', t) - 6P(r, t)] - \theta \delta_{z,0} P(r, t) \quad (\text{A1})$$

where δt denotes the microscopic diffusion time step, $\tilde{D} = D\delta t / \Delta^2$ is the effective diffusion coefficient for the underlying lattice (which we take to be cubic for simplicity) and $r = (x, y, z)$ represents the position of the particle in the three-dimensional space. The first term in Eq. A1 is simply the diffusion of the particle away from the surface, and the last term represents the adsorption at the surface that occurs with probability θ .

Since the space coordinates are clearly statistically independent here, the solution to Eq. A1 can be written in the form of a product, $P(x, y, z; T) = G_1(x; T)G_2(y; T)G_3(z, Z; T)$. Upon substitution in Eq. A1, we find, of course, that G_1 and G_2 satisfy the simple one-dimensional diffusion equation (without any adsorption), and only G_3 is modified by the adsorption term. The complete probability distribution may then be written as

$$P(x, y, z; T) = \frac{1}{2\pi DT} \exp\left(-\frac{x^2 + y^2}{2DT}\right) G_3(z, Z; T) \quad (\text{A2})$$

The rate of adsorption of the ligand at the surface ($z=0$) is simply $\tilde{P}(x, y; T) = -\partial_z P|_{z=0}$, and from Eq. A2, we infer that the derivative acts only on the function G_3 . For a dissociated ligand, the initial position on the z -axis is $z=\Delta$. Hence, the absorption rate becomes

$$\tilde{P}(x, y; T) = \frac{1}{2\pi DT} \exp\left(-\frac{x^2 + y^2}{2DT}\right) C_\theta(\Delta, T) \quad (\text{A3})$$

where $C_\theta(\Delta, T) = -\partial G_3 / \partial Z|_{z=0}$ is the rate (i.e., the probability per unit diffusion time step) that a particle diffusing in one dimension that started at $z = \Delta$ at $t = 0$ is absorbed at the origin $z = 0$ at a later time $T > 0$. This probability is calculated in a straightforward manner by making use of the independence of the successive returns of a random walk to its starting point, as has been done in Sec. 3.1.

The total probability of re-adsorption of a ligand, averaged over all space, is thus

$$\gamma(t) = \beta \int_0^t d\tau p(\tau) \int dx dy \tilde{P}(x, y; t - \tau) \quad (\text{A4})$$

After substituting Eq. A3 into Eq. A4 and performing the trivial spatial averaging, we finally arrive at Eq. 3.

Appendix B

Let us define the dimensionless variables $T=\beta t$ and $\lambda=s/\beta$, so that the Laplace transform $\tilde{p}(s)=\frac{1}{\beta}F(\lambda)$, where $F(\lambda)=\int \tilde{p}(T)e^{-\lambda T}dT$ and $\tilde{p}(T)\equiv p(\beta T)$. From Eq. 4, we then find that:

$$F(\lambda)=\frac{p(0)}{\lambda+G(\lambda)} \quad (\text{B1})$$

where $G(\lambda)=1-\tilde{C}_\theta(\beta\lambda)$. When δ is small, we approximate $e^{-2\sqrt{\delta}s}\approx 1-2\sqrt{\delta}s$ in Eq. 9, which leads to:

$$G(\lambda)\approx\frac{2\sqrt{\tilde{\beta}\lambda}}{2\sqrt{\tilde{\beta}\lambda}+\theta(1-2\sqrt{\tilde{\beta}\lambda})}\rightarrow\frac{2\sqrt{\tilde{\beta}\lambda}}{2\sqrt{\tilde{\beta}\lambda}+\theta} \quad (\text{B2})$$

when θ is small (where $\tilde{\beta}=\beta\delta$ is a dimensionless constant).

Clearly, two regimes can be identified here: If $\theta\gg\sqrt{\tilde{\beta}}$ it is safe to approximate $G(\lambda)\approx(2/\theta)\sqrt{\tilde{\beta}\lambda}$ (except when $\lambda\gg 1$, but this corresponds to very small times $t\ll\delta$, so this case can be ignored here). Upon inversion, this leads to the expression in Eq. 11.

On the other hand, if $\theta\ll\sqrt{\tilde{\beta}}$, we may use the binomial expansion $G(\lambda)=1-\theta/2\sqrt{\tilde{\beta}\lambda}+O(\theta^2)$. Substitution in Eq. B1 yields:

$$F(\lambda)=\frac{p(0)}{\lambda+1}+\frac{\theta p(0)}{2(\lambda+1)^2\sqrt{\tilde{\beta}\lambda}}+O(\theta^2) \quad (\text{B3})$$

The first term (upon inversion of the Laplace transform) gives the exponential decay without rebinding, and the subsequent terms are the corrections due to rebinding, in powers of the coverage fraction θ .

Can this regime be reached in a hypothetical SPR experiment (i.e., can we recover exponential decay by simply reducing the surface coverage of receptors)? Our answer, based on the preceding analysis, is that it is unlikely but dependent on the system and the affinities of interaction. Because of the microscopic nature of the time scale δ , the parameter $\tilde{\beta}$ would be very small in experiments (for the estimates in Sec.4, we used $\tilde{\beta}\approx 10^{-14}$ only!) meaning that the surface coverage and/or the adsorption probability required would have to be extremely small ($\theta\leq 10^{-7}$). Such a small coverage would likely lead to signal to noise issues.

Heparin level (μM)	Fit parameter c_H (s^{-1})	$\theta_H / \theta_0 = \sqrt{c_0 / c_H}$
0.0	$1.9 \times 10^{-5} = c_0$	1.0000
1.8	2.9×10^{-4}	0.2559
3.6	4.1×10^{-4}	0.2140
5.4	5.9×10^{-4}	0.1934
10.8	8.0×10^{-4}	0.1495

TABLE 1: Fit parameters to SPR experimental data for various heparin concentrations. Note that the ‘effective coverage’ decreases with the heparin concentration (since the ligand bound to heparin is unavailable for binding to surface proteins), but the drop is much less rapid than a prediction based on complete equilibration between the heparin and IGF concentrations would suggest.

Figure legends:

FIG 1: (A) A schematic diagram of the SPR experimental set-up showing the attached ligands (IGF-I) available for binding to the IGFBP-3 in solution (B) Representative association-dissociation plot of IGFBP-3 (20 nM) for surface-coupled IGF-I under flow conditions. The arrow labeled PBST indicates when the fluid was changed from IGFBP-3 in PBST to only PBST, thus initiating the dissociation phase.

FIG 2. (A). Representative plot of dissociation phase data for IGFBP-3 under flow and non-flow conditions, both normalized to peak value. (B) Representative plot of association phase data for IGFBP-3 (50 nM) +/- heparin (200 nM) or heparin alone to IGF-I (off-line coupling) under flow conditions.

FIG.3. Representative data for dissociation phase of IGFBP-3 from IGF-I for PBST (buffer alone) or heparin (30 μ M) in PBST for duplicate runs of each on the same chip normalized to the individual time 0 value. The data is representative of multiple runs performed on six independent chips.

FIG 4. Comparison of dissociation data in the presence of heparin (30 μ M) for two different levels of surface coupled IGF-I (on-line coupling): (\diamond) \sim 4 pixels of surface coverage and (+) \sim 12 pixels of surface coverage. This observation is consistent with the mean-field calculation in Sec. 3.1 in the text. Results for other heparin concentrations, as well as runs without heparin, showed similar trends.

FIG 5. Normalized dissociation curve from simulations of the lattice model for two different surface protein densities. The initial bound fraction $p(0)$ is 0.25 in both cases, and the dissociation rate is $\tilde{\beta} = 10^{-5}$. The thin lines indicate optimal fits using Eq. (11), with $c = 0.01$ for $\theta = 0.1$ and $c = 0.0004$ for $\theta = 0.5$. The corresponding theoretical values are $c = 0.012$ and $c = 0.00048$. The results represent averages over 20 different starting configurations.

FIG 6. The effect of reducing the dissociation coefficient relative to the surface coverage (which is fixed at 1% here) in the simulations. We observe that when the dissociation rate is high, the temporal decay becomes effectively exponential (compare with the dashed exponential curve) in accordance with the mean-field calculations in Appendix B. As β is reduced, rebinding is increasingly important, and the dissociation slows down. The results were averaged over 20 different starting configurations.

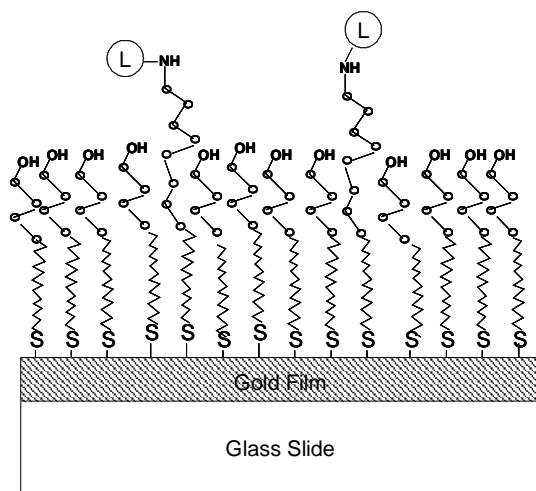
FIG 7. Simulation dissociation curves for two small coverage fractions, 0.5% and 1% of the surface area. The dissociation rate is $\tilde{\beta} = 10^{-5}$.

FIG 8. The same data as in Fig. 7 is plotted on a logarithmic scale. This plot shows the cross-over to the power-law regime mentioned in Sec. 3.1. The straight line is a fit function $f(T) = T^{-1/2}$.

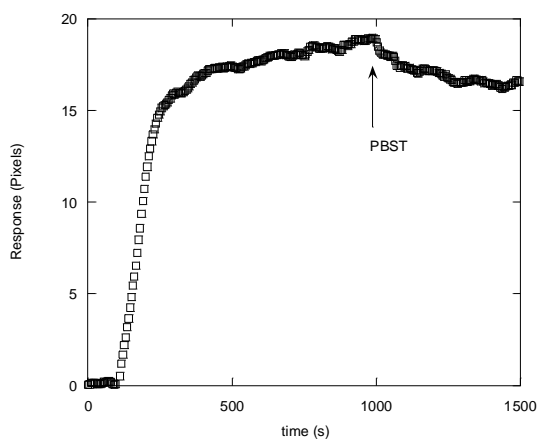
FIG.9. Comparison of mean-field theory with experimental SPR data (\diamond) for IGFBP-3 dissociation from IGF-I in the absence of heparin. The thin line represents the best fit using Eq.(11), with $c = 1.9 \times 10^{-5} \text{ s}^{-1}$. The deviation from the mean-field prediction at $t > 200 \text{ s}$ is likely due to the finite height of the experimental system (ligands are reflected back towards the binding surface). The experimental data was averaged over two different runs on the same IGF-I coupled chip and is representative of averaged data from six separate chips.

FIG.10. Comparison of mean-field theory with IGFBP-3 dissociation SPR data in the presence and absence of heparin (concentration of heparin indicated on figure by experimental values). The lines represent the fitting curves using Eq.(11), with fit parameters $c = 4.1 \times 10^{-4} \text{ s}^{-1}$ and $c = 5.9 \times 10^{-4} \text{ s}^{-1}$ respectively for $3.6 \text{ }\mu\text{M}$ and $5.4 \text{ }\mu\text{M}$ heparin .

FIGURES

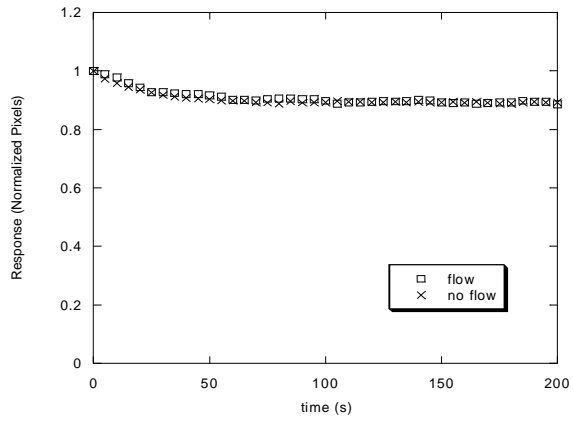


(A)

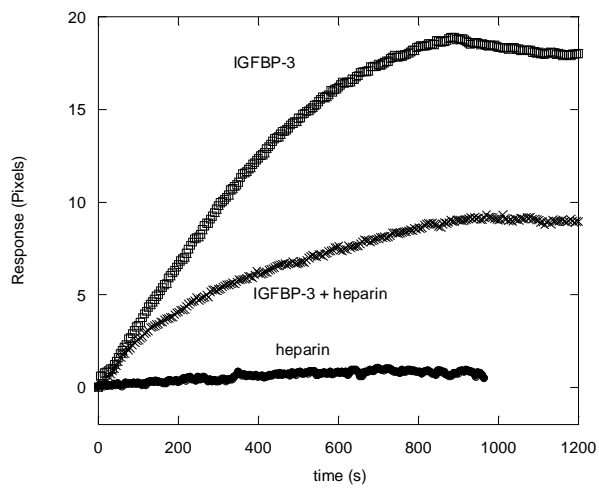


(B)

FIG 1.



(A)



(B)

FIG 2.

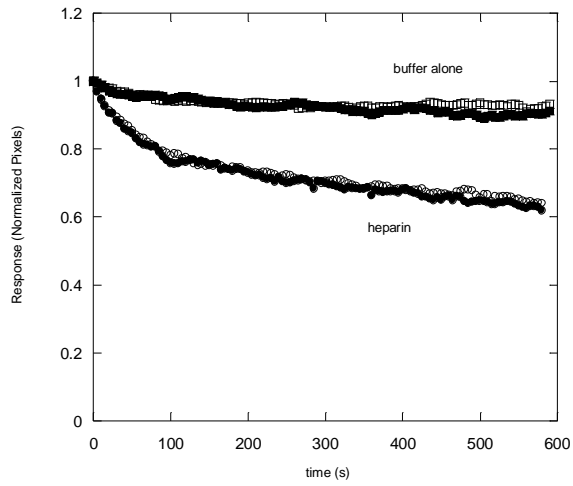


FIG 3.

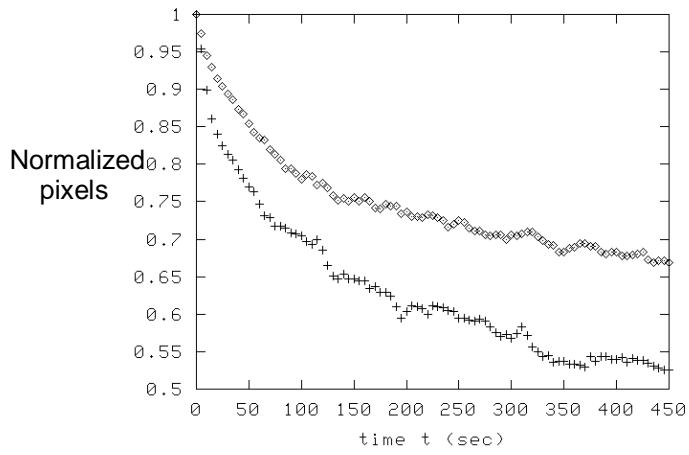


FIG 4.

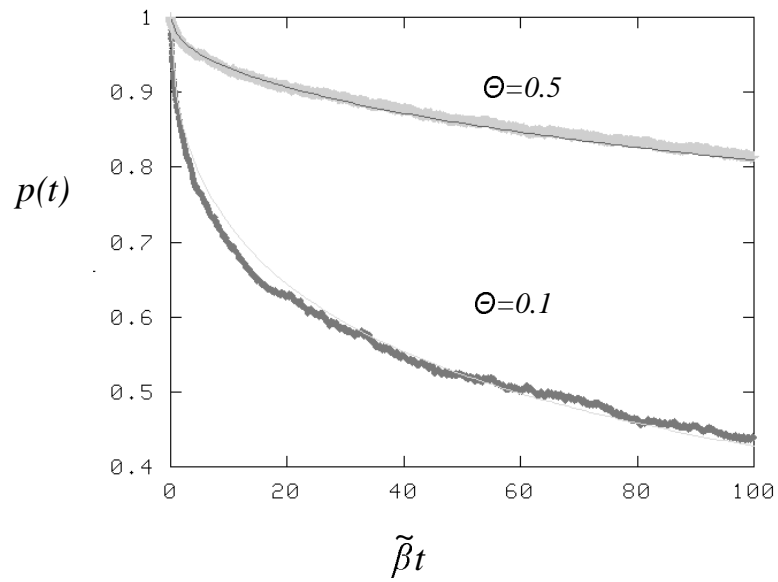


FIG 5.

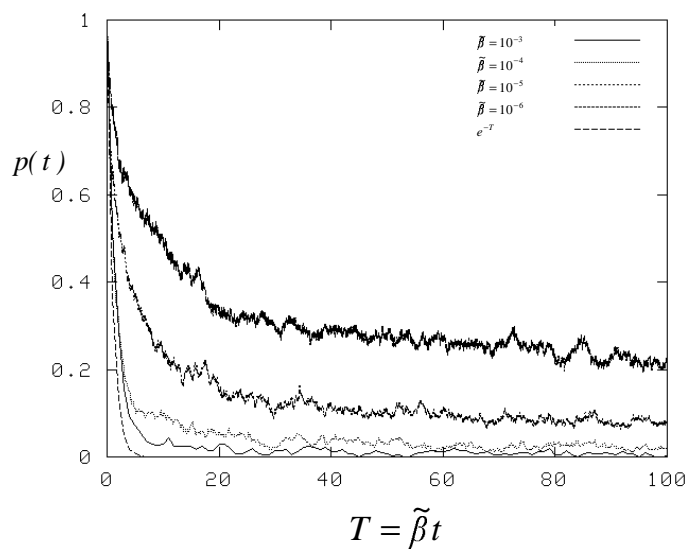


FIG 6.

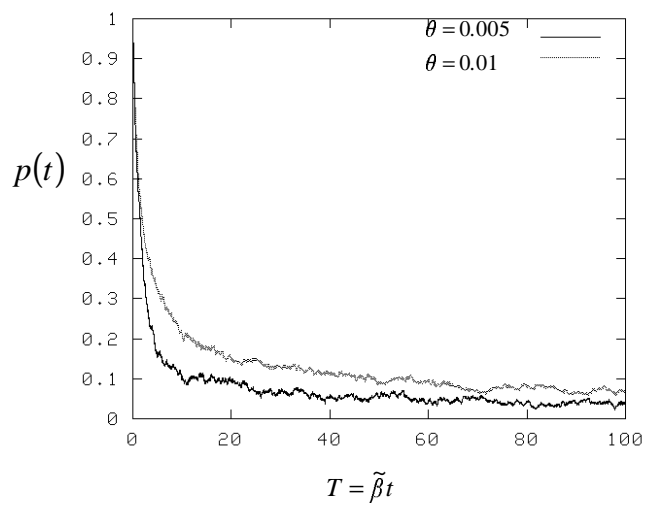


FIG 7.

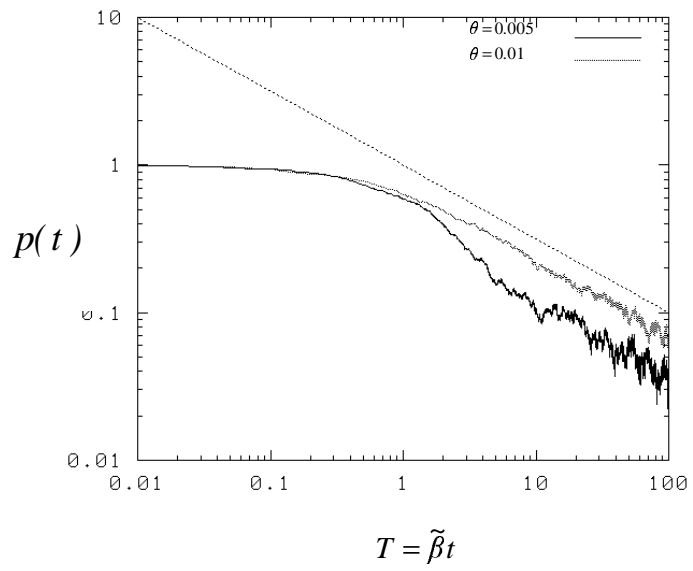


FIG 8.

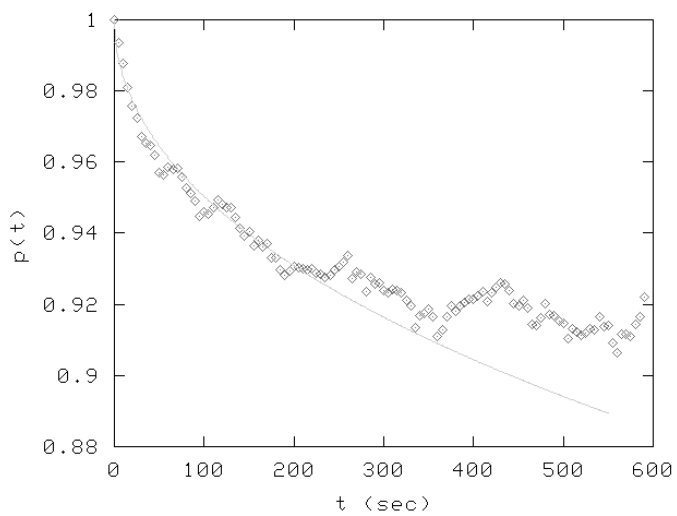


FIG 9.

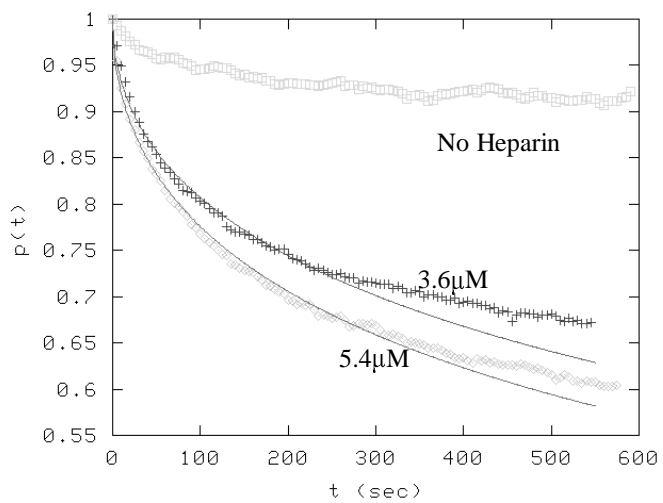


FIG 10.